UDC 539.4

Fiber Laser Welding of Dual-Phase and Bake-Hardened Steels

P. Ďvec,[1] A. Schrek,[2] and T. Csicsó[3]

Slovak University of Technology, Bratislava, Slovakia

[1] pavol.svec@stuba.sk

[2] alexander.schrek@stuba.sk

[3] tomas.csicso@stuba.sk

Microstructural changes and microhardness profiles of laser-welded dual-phase DP600 and bake-hardened 220BH steels were evaluated. The joints of these steels were butted with different welding parameters. They exhibited the microstructural changes, from ferrite and martensite in dual-phase steels or ferrite in bake-hardened steels to acicular ferrite, bainite and martensite in the fusion and heat-affected zones of the weld joints. As a result of welding, microhardness increases significantly in the fusion zones and even more in the heat-affected zones near DP600 steel.

Keywords: dual-phase steels, bake-hardened steels, fiber laser welding, microstructure, microhardness.

Introduction. Recent legislation provides for a reduction in greenhouse gas emissions and fuel consumption to protect our precious environment, mitigate man-made global warming, and decrease costs. Automotive industry is also constantly seeking efficient methods to manufacture vehicles from lighter materials or materials of higher strength and ductility so as to reduce the vehicle weight with guaranteeing improved occupant safety. The materials used for automotive applications must be easily formable, weldable, and repairable. Dual-phase (DP) steels, which normally contain dispersed islands of martensite in the ferritic matrix, satisfy these requirements fairly well [1–4]. The ductility arises from ferrite while martensite accounts for the strength, and with an increase in the volume fraction of martensite, the strength of DP steels grows and the ductility decreases. Ferrite-martensite DP steels are usually produced by intercritical annealing followed by rapid cooling. Intercritical annealing results in small pools of austenite formed in the ferritic matrix, which subsequently transform into martensite on rapid cooling. The austenite-to-martensite transformation, accompanied by volume expansion, leads to the penetration of mobile dislocations into the surrounding ferritic matrix. The mobility of these dislocations is responsible for a high initial strain hardening rate and continuous deformation in DP steels. The properties of DP steels can be utilized in "tailor-made" welded blanks, and these can consist of DP and bake-hardened (BH) steels. The welded blanks of these steels enable an adaptation to different local loading conditions on forming and crash [2, 5, 6].

Laser beam welding has become one of the important techniques widely used in modern industries due to its superior properties, such as a high welding speed, low thermal distortion, ease of automation, thin and small weld seams, and the possibility of on-line quality control during the process. Nd:YAG and CO_2 lasers are commonly used in ship building, defence, and aerospace sectors. Recent developments of solid state lasers include disk, diode, and fiber lasers with high wall-plug efficiency and superior beam quality. Laser welding of dissimilar materials has received wide acceptance from automotive, power, chemical, nuclear, and aerospace industries [7, 8]. The quality of weld joints is significantly affected by the defects generated in welding of dissimilar materials. Advanced manufacturing would require a certain special combination of material properties, in this connection, the

demand for welding of dissimilar metals is continuously increasing. The products consisting of different metals and compositions offer a designer and production engineer more versatile properties, greater flexibility and lower costs as compared to expensive and scarce materials and components manufactured from similar entities [9–11].

Experimental Procedure. Dual-phase DP600 and bake-hardened 220BH steels were chosen for laser welding. Their chemical composition and mechanical properties are cited in Tables 1–3. The experimental steels differ in their maximum allowable concentrations ($c_{\max}$) of carbon and alloying elements. The DP steel has a higher content of these elements, which results in its higher strength but lower plasticity as compared to the BH steel.

T a b l e 1

Chemical Composition of Dual-Phase DP600 Steel

Element	C	Si	Mn	P	S	V	Al	B	Cr+Mo	Nb+Ti
$c_{\max}$, wt.%	0.17	0.8	2.2	0.08	0.015	0.2	2.0	0.005	1.0	0.15

T a b l e 2

Chemical Composition of Bake-Hardened 220BH Steel

Element	C	Si	Mn	P	S	Nb	Ti	Al
$c_{\max}$, wt.%	0.1	0.5	0.7	0.08	0.025	0.09	0.12	0.1

T a b l e 3

Mechanical Properties of Steels

Steel	Tensile strength (MPa)	Proof strength (MPa)	Minimal elongation at $L_0 = 80$ mm (%)
DP600	600	340–420	20
220BH	320–400	220–280	32

The blanks of both steels with a zinc coating of 100 g/m^2 and 1.2 mm thick were welded with an Nd:YAG YLS 5000 fiber laser welding machine with a maximum beam power of 5 kW and wavelength of 1.06 μm. The fiber diameter was 0.1 mm, and a focal distance was 150 mm. Welding experiments were conducted on sheets 200 mm long and 100 mm wide across the longitudinal edge. Prior to welding abutting surfaces were cleaned with a steel wire brush and acetone. The macrostructure of laser-welded surfaces produced with different welding parameters was investigated using a Zeiss stereomicroscope. The microstructure was studied on the specimens cut out from the weld joints with an Axiovert 40MAT light microscope and JEOL IT300 scanning electron microscope. Microhardness profiles were analyzed on the transverse sections of the weld bead center parallel to the sheet surfaces using Vickers indentation.

Results and Discussion. Butt weld joints were made at five different beam power (P) values, welding speeds (v), and calculated heat inpust (P/v), summarized in Table 4.

The face and root of a DP600–220BH laser weld are exemplified in Fig. 1. The weld joint, produced at the beam power of 1500 W and welding speed of 30 mm/s, displays a particular splash and small pinholes on the weld root. The oxidation zones 2.5 mm wide on the face and 4 mm wide on the root of the weld are visible.

Table 4

Laser Welding Parameters for DP600–220BH Joints

Weld number	Beam power (W)	Welding speed (mm/s)	Heat input (W/(mm·s))
1	900	10	90.0
2	1500	30	50.0
3	2200	50	44.0
4	2760	70	39.4
5	4000	100	40.0

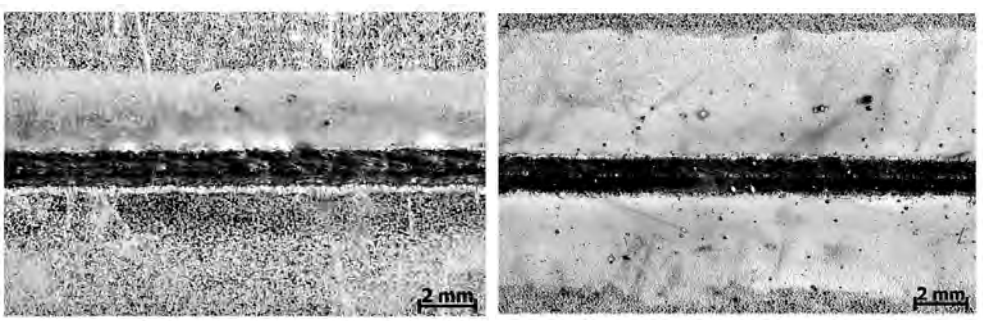

a b

Fig. 1. Macrostructure of the face (a) and root (b) of a DP600–220BH joint ($P = 1500$ W, $v = 30$ mm/s).

The specimens welded at different parameters were similar and did not have any macroscopic defects. Increased beam powers and welding speeds resulted in lower heat inputs and higher cooling speeds accompanied by a more intensive splash and larger pinholes but narrower weld widths.

Microstructure Evolution. The microstructures of both base metals (BM) are depicted in Figs. 2 and 3. The microstructure of DP steel in Fig. 2 consists of martensite islands in the ferritic matrix. The average grain sizes of DP steel measured by image analysis were 7 μm for ferrite equiaxed grains and 1 μm for martensite grains. The fractions of ferrite and martensite are 75 and 25 vol.%, respectively. The BH steel in Fig. 3 has the ferrite microstructure with an average grain size of 10 μm, which is slightly higher than that of the DP steel.

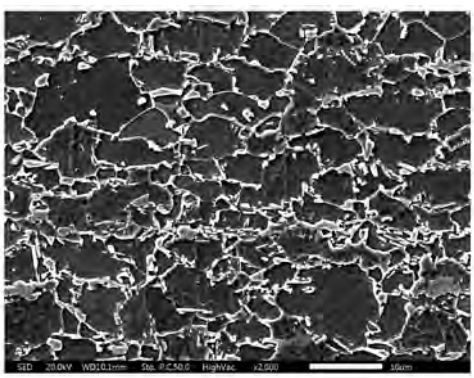

Fig. 2. Microstructure of DP600 steel.

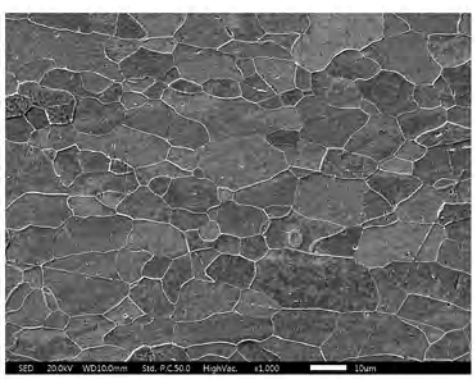

Fig. 3. Microstructure of 220BH steel.

Joints welded at different parameters consisted of the same microconstituents but with their different fractions. Typical microstructural changes during laser welding are demonstrated in Fig. 4, with the joint welded at the beam power of 1500 W and welding speed of 30 mm/s, as is seen through a light microscope. It is typical microstructural changes from ferrite and martensite or ferrite in the base metal to ferrite, bainite, and martensite in the fusion zone (FZ).

The FZ microstructure viewed through an electron microscope is shown in Fig. 5. The FZ contained a large amount of acicular ferrite and small areas of martensite and bainite. The formation of those nonequilibrium microconstituents in FZ was the result of rapid cooling of the weld pool containing a relatively higher content of alloying elements, like Mn, Cr, Mo, Al, etc. (Tables 1 and 2). More martensite and bainite were revealed in the joints produced at higher beam powers and welding speeds as compared to their lower values.

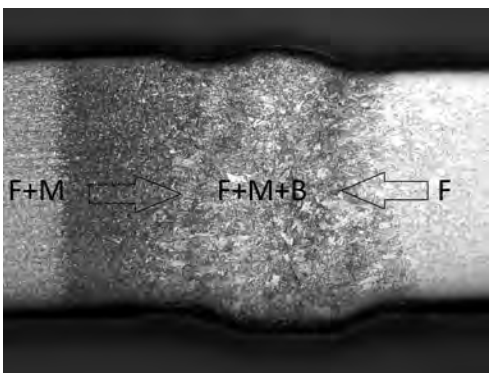

Fig. 4

Fig. 5

Fig. 4. Typical microstructural changes during laser welding process (F – ferrite, M – martensite, B – bainite, $P = 1500$ W, and $v = 30$ mm/s).
Fig. 5. Fusion zone of a DP600–220BH joint.

The microstructures of both heat-affected zones (HAZ) were different (Figs. 6 and 7). As DP600 steel contains a larger amount of alloying elements in comparison with 220BH steel, the HAZ microstructure near the former consisted mainly of lath-shaped micro-consituents built in packets. These packets can be martensite or bainite (Fig. 6). The HAZ microstructure near 220BH steel consisted mainly of ferrite and acicular ferrite, as can be seen in Fig. 7.

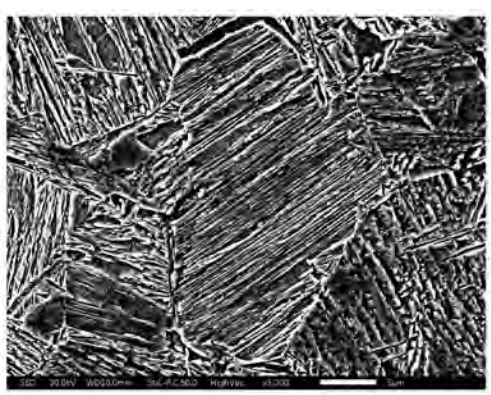

Fig. 6. HAZ microstructure near DP600 steel.

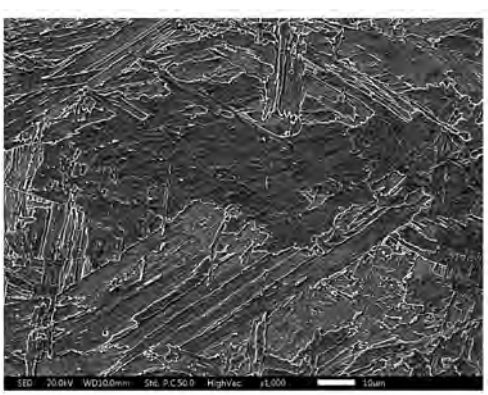

Fig. 7. HAZ microstructure near 220BH steel.

Microhardness Profiles. Microhardness profiles of a DP600–220BH joint can be seen in Fig. 8. The Vickers microhardness was determined at the load of 50 and 100 g, dwell time of 15 s, and indentation distances of 0.1 or 0.05 mm.

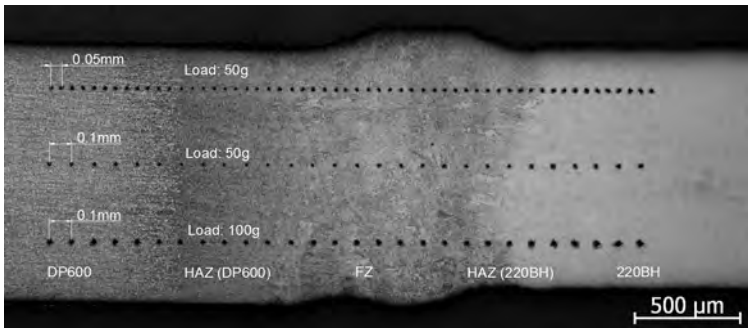

Fig. 8. Microhardness profiles of a DP600–220BH joint ($P = 1500$ W, $v = 30$ mm/s).

The microhardness profiles of DP600–220BH joints welded at both the highest [90 W/(mm · s)] and lowest [40 W/(mm · s)] heat inputs are presented in Figs. 9 and 10. The microhardness profiles show microhardness variations measured across FZ, HAZ, and BM. The highest heat input corresponds to the beam power of 900 W and welding speed of 10 mm/s, and the lowest heat input was calculated for the beam power of 4000 W and welding speed of 100 mm/s. Both microhardness profiles are characterized by similar asymmetric shapes but by slightly different maximum values in particular joint zones. The microhardness values of those zones correspond to their microstructure. The maximum microhardness values were measured in the joints welded at minimum heat inputs, which resulted in maximum cooling speeds. The widths of both FZ and HAZ decreased with decreasing heat inputs (Figs. 9 and 10).

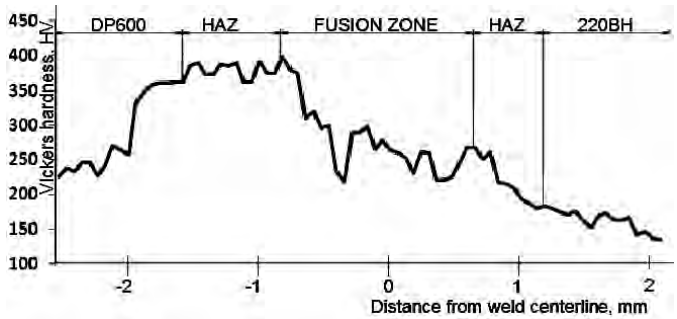

Fig. 9. Microhardness profile of a DP600–220BH joint ($P = 900$ W, $v = 10$ mm/s).

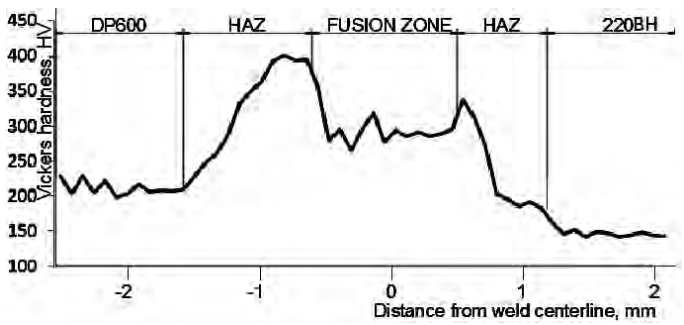

Fig. 10. Microhardness profile of a DP600–220BH joint ($P = 4000$ W, $v = 100$ mm/s).

The 220BH steel base metal had the lowest microhardness, below 150 HV, and this value represents the ferrite microstructure of this steel (Fig. 3). The microhardness of DP600 steel was 220 HV, which is in good agreement with the dual-phase ferrite and martensite microstructure (Fig. 2). The microhardness of 300 HV measured in FZ confirmed the formation of bainite and martensite in FZ. A major difference in the microhardness of both HAZs is in good agreement with their microstructure. The HAZ near DP600 steel contained the greatest amount of hard lath-shaped microconstituents (Fig. 6) and reached the highest microhardness, above 400 HV. The microhardness in HAZ near 220BH steel was below 300 HV (Fig. 7) because of the formation of softer microconstituents as compared to HAZ near DP600 steel.

Conclusions. Laser welding of dual-phase DP600 and bake-hardened 220BH steels at different parameters was evaluated. The beam power varied over the range of 900–4000 W and the welding speed changed from 10 to 100 mm/s. The welding parameters effected the microstructure and microhardness of butt joints. The FZ contained a great amount of acicular ferrite and small areas of martensite and bainite. The formation of these nonequilibrium microconstituents was the result of rapid cooling of the weld pool containing a relatively higher content of alloying elements. The HAZ microstructure near DP600 steel consisted mainly of lath-shaped microconsituents built in packets, and the HAZ microstructure near 220BH steel consisted mainly of ferrite and acicular ferrite. The microhardness profiles of all specimens were of asymmetric shape and consistent with their microstructure. The highest microhardness, above 400 HV was measured in HAZ near DP600 steel with the highest fraction of hard lath-shaped microconstituents.

Acknowledgments. This study was supported by the Slovak Research and Development Agency under contract No. APVV-0281-12.

1. H. Gong, S. Wang, P. Knysh, and Y. P. Korkolis, “Experimental investigation of the mechanical response of laser welded dissimilar blanks from advanced- and ultra-high-strength steels,” *Mater. Design*, **90**, 1115–1123 (2016).
2. D. C. Saha, D. Westerbaan, S. S. Nayak, et al., “Microstructure-properties correlation in fiber laser welding of dual-phase and HSLA steels,” *Mater. Sci. Eng. A*, **607**, 445–453 (2014).
3. N. Farabi, D. L. Chen, and Y. Zhou, “Microstructure and mechanical properties of laser welded dissimilar DP600/DP980 dual-phase steel joints,” *J. Alloys Compd.*, **509**, 982–989 (2011).
4. Y. X. Chen, C. D. Yang, X. J. Wang, and H. B. Chen, “Evaluation of metal-active gas double-sided double-power arc welded joints of high-strength low-alloy steel,” *Strength Mater.*, **47**, No. 1, 164–169 (2015).
5. J. Meðko, A. Zrak, K. Mulczyk, and S. Tofil, “Microstructure analysis of welded joints after laser welding,” *Manuf. Technol.*, **14**, No. 3, 355–359 (2014).
6. S. Krajewski and J. Nowacki, “Dual-phase steels microstructure and properties consideration based on artificial intelligence techniques,” *Arch. Civil Mech. Eng.*, **14**, No. 2, 278–286 (2014).
7. M. S. Weglowski, K. Kwiecinski, K. Krasnowski, and R. Jachym, “Characteristics of Nd:YAG laser welded joints of dual phase steels,” *Arch. Civil Mech. Eng.*, **9**, No. 4, 85–97 (2009).
8. N. Farabi, D. L. Chen, J. Li, et al., “Microstructure and mechanical properties of laser welded DP600 steel joints,” *Mater. Sci. Eng. A*, **527**, 1215–1222 (2010).
9. J. Vinas and M. Abel, “Analysis of laser welds on automotive steel sheets,” *Mater. Sci. Forum*, **818**, 239–242 (2015).

10. M. Merklein, M. Johannes, M. Lechner, and A. Kuppert, “A review on tailored blanks – Production, applications and evaluation,” *J. Mater. Process. Technol.*, **214**, No. 2, 151–164 (2014).

11. HanSur Bang, HeeSeon Bang, M. J. Na, et al., “Application of Taguchi approach to optimize laser-arc hybrid welding parameters of galvanized steel,” *Strength Mater.*, **48**, No. 1, 146–151 (2016).

Received 10. 08. 2016